THE JOURNAL OF PHYSICAL CHEMISTRY LETTERS
A JOURNAL OF THE AMERICAN CHEMICAL SOCIETY

pubs.acs.org/JPCL

Letter

Theoretical Design of Optimal Molecular Qudits for Quantum Error Correction

A. Chiesa,* F. Petiziol, M. Chizzini, P. Santini, and S. Carretta*

Cite This: *J. Phys. Chem. Lett.* 2022, 13, 6468−6474

Read Online

ACCESS | Metrics & More | Article Recommendations | Supporting Information

ABSTRACT: We pinpoint the key ingredients ruling decoherence in multispin clusters, and we engineer the system Hamiltonian to design optimal molecules embedding quantum error correction. These are antiferromagnetically coupled systems with competing exchange interactions, characterized by many low-energy states in which decoherence is dramatically suppressed and does not increase with the system size. This feature allows us to derive optimized code words, enhancing the power of the quantum error correction code by orders of magnitude. We demonstrate this by a complete simulation of the system dynamics, including the effect of decoherence driven by a nuclear spin bath and the full sequence of pulses to implement error correction and logical gates between protected states.

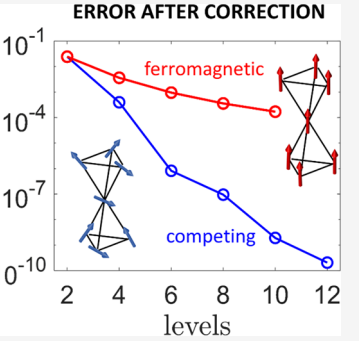

Quantum computers promise to outclass classical digital devices in the solution of currently intractable problems. However, none of the existing technologies[1−10] can suppress errors on each computational qubit to the level required to achieve a real quantum advantage. The only way to get around this hurdle is by replacing two-level qubits with more complex logical units, supporting quantum-error correction (QEC). Each of these units is usually represented by a large collection of qubits,[11,12] at least 10^3−10^4 to get, for example, a likely success in factoring a 2000-bit number.[13] Even for the most advanced platforms, this makes the actual manipulation of the resulting register practically unfeasible and hence still represents an almost prohibitive goal.

Molecular spin systems offer a new alternative perspective, which can overcome major limitations of qubit-based approaches. In particular, they are typically characterized by many electronic and nuclear spin states (i.e., a *qudit* structure), which can be coherently manipulated through microwave or radio frequency pulses.[14−20] We have recently shown that these qudits can be exploited to embed QEC within a single object, thus greatly simplifying its actual implementation.[21,22] The $2S + 1$ states of a spin S ion (for which several examples exist[23−29]) provide the chemically simplest implementation, which already ensures a gain in the lifetime of a quantum memory.[21,22] By increasing S, and hence the number of levels in the encoding, one could in principle increase the correcting capacity of the code.

However, the dramatic growth of decoherence with S yields only a limited gain in actually performing quantum error correction. Moreover, quantum gates between logical states encoded in spin S qudits are not allowed. Instead, to implement complex algorithms, logical units must display errors not increasing significantly with the system size and must support gates between encoded states.

Here we show that both these challenging tasks can be achieved by fully unleashing the chemical tunability of our molecular hardware, which constitutes its fundamental advantage but was not exploited to date. In particular, we theoretically design optimal molecules showing a large number of low-energy states, for which decoherence is strongly suppressed and does not grow with the system size. This allows us to increase the number of levels in the encoding without being limited by the corresponding loss of coherence. As a result, the correcting power of the code is largely enhanced, by orders of magnitude compared to the case of a spin S system. The optimal units are represented by multispin molecules with antiferromagnetic competing exchange interactions,[30−34] leading to several magnetically similar multiplets at low energy. As a consequence, superpositions of all the states belonging to these multiplets are substantially protected from decoherence in a way that does not worsen by adding levels.

We demonstrate this by considering a 7-spin molecule in a bath of nuclear spins, driving decoherence at low temperature. We numerically compute the resulting effect of dephasing on the lowest energy levels, and we derive code words exploiting superpositions of these levels. We then compare the perform-

Received: May 26, 2022
Accepted: July 7, 2022

ance of the QEC code for the same molecular structure with competing versus ferromagnetic exchange interactions (producing a ground spin S multiplet), finding an impressive gain for the former. Finally, we exploit another peculiar feature of the designed molecule, namely, the possibility to induce direct transitions between all the selected energy levels, to actually implement quantum error correction and quantum gates between encoded states.

Design of Molecular Nanomagnets with Suppressed Decoherence. To design optimal molecular systems, we first pinpoint the crucial ingredients related to the spin structure of the eigenstates driving decoherence and then identify the requirements to keep them under control. The dominant source of decoherence in molecular nanomagnets at low temperature is the hyperfine coupling of the system spins with the surrounding nuclear spins, while phonon-mediated processes are practically negligible.[22,23] Starting from the microscopic system-bath Hamiltonian and from the system eigenstates, we derive in the Supporting Information a master equation describing the dynamics of the system in the secular and Born−Markov approximations. This yields a decay of the system coherences $\rho_{\mu\nu}(t) = \exp(-\gamma_{\mu\nu}t)\rho_{\mu\nu}(0)$ with decay rates

$$\gamma_{\mu\nu} = \sum_{jj'=1}^{7} C_{jj'}^{zz}[-2\langle\mu|s_j^z|\mu\rangle\langle\nu|s_{j'}^z|\nu\rangle + \langle\mu|s_j^z|\mu\rangle\langle\mu|s_{j'}^z|\mu\rangle + \langle\nu|s_j^z|\nu\rangle\langle\nu|s_{j'}^z|\nu\rangle] \quad (1)$$

Here, ρ is the density matrix, $|\mu\rangle$ and $|\nu\rangle$ are system eigenstates, and the coefficients $C_{jj'}^{zz}$ contain sums over products of dipolar couplings between local system and bath spin operators.[49] Although neglecting the details of the spin-bath dynamics, this approach captures the dramatic impact of the spin structure of the eigenstates on the dephasing process, the key ingredient for the design of optimal molecules. Indeed, as demonstrated in the Supporting Information, the detailed description of the bath dynamics does not qualitatively alter our main conclusions.[50]

The key factors ruling decoherence in eq 1 are weighted differences between expectation values of local spin operators on different eigenstates. In order to suppress decoherence and in particular to avoid its growth when additional states are considered, the values of $\langle\mu|s_j^z|\mu\rangle$ and their variation within the examined set of eigenstates must be as small as possible. This suggests as ideal candidates antiferromagnetically coupled systems with competing exchange interactions (i.e., close to spin frustration), which are expected to display several "magnetically similar" low-energy multiplets, i.e., characterized by similar and small values of $\langle\mu|s_j^z|\mu\rangle$.

Quasi-frustration is typically associated with the presence of triangular units with antiferromagnetic coupling in the molecule. For example, a single triangle of $s_i = 1/2$ spins may provide two low-energy multiplets with small total spin $S = 1/2$. This is not enough for the present study, where we want to compare the performance of the QEC protocol across a broad range of qudit sizes. Thus, we consider a bigger molecule whose structure remains as simple as possible but which can accommodate a larger number of suitable low-energy multiplets: two corner-sharing tetrahedra of antiferromagnetically coupled spins (Figure 1a), a structure analogous to that of the Ni_7 cluster.[30] A simple choice yielding a large number of low-lying multiplets is six spins $s_i = 1/2$ ($i = 1, ..., 6$) and a spin

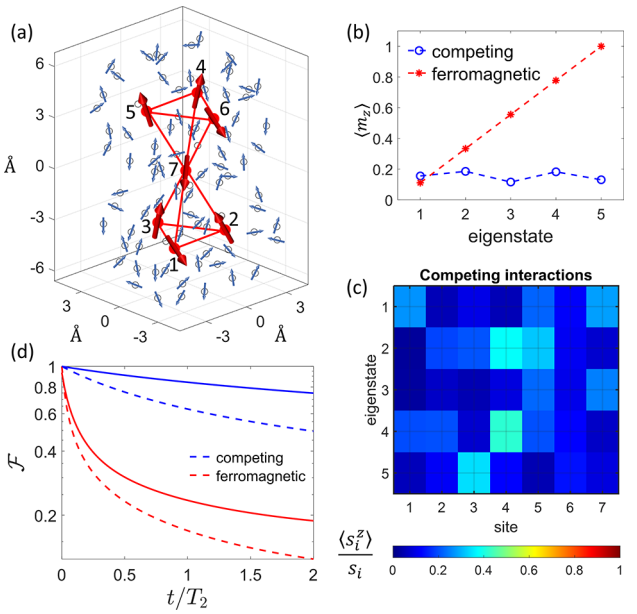

Figure 1. Suppression of decoherence in a multispin molecule with competing interactions. (a) Hypothetical multispin cluster consisting of six $s_i = 1/2$ and a spin 3/2 ion in the center (such as Cu^{2+} and Cr^{3+}, red arrows), arranged in a double-tetrahedron structure similar to Ni_7.[30] Calculations are performed by assuming $J_{1,2} = 1.14$ meV, $J_{1,3} = J_{2,3} = 1.15$ meV, $J_{4,5} = 1.13$ meV, $J_{4,6} = J_{5,6} = 1.10$ meV, $J_{1,7} = 0.82$ meV, $J_{2,7} = 0.85$ meV, $J_{3,7} = 0.87$ meV, $J_{4,7} = 0.83$ meV, $J_{5,7} = 0.81$ meV, $J_{6,7} = 0.90$ meV, and $D_{i,j} = J_{i,j}/10$. The system is surrounded by a random distribution of nuclear spins 1/2 (blue arrows) with minimal distance 2 Å centered around each ion, ruling decoherence. (b) Comparison between the average expectation values of local spin operators $\langle m_z\rangle = \sum_i \langle s_i^z\rangle/7s_i$ in the case of competing (blue) vs ferromagnetic (red) exchange interactions in the molecular structure shown in panel a, for different sites and eigenstates (one per each of the lowest 5 Kramers doublets). (c) Distribution of expectation values of local spin operators $\langle s_i^z\rangle/s_i$ on different sites and eigenstates of the cluster (a) with competing interactions. The much larger variation of $\langle m_z\rangle$ within the $S = 9/2$ ground multiplet in panel b is reflected (panel d) by the impressive reduction of the fidelity for a state prepared in an initial generic uniform superposition (dashed lines) or in the encoded state $(|0_L\rangle + |1_L\rangle)/\sqrt{2}$ (solid). Here $\mathcal{F} = \langle\psi_0|\rho|\psi_0\rangle$, where $|\psi_0\rangle$ is the initial state and ρ is the system density matrix subject to decoherence for a time t.

$s_7 = 3/2$ (red spheres and arrows) at the shared corner. The system is described by the following spin Hamiltonian:

$$H = \sum_{i>j} J_{i,j}\mathbf{s}_i\cdot\mathbf{s}_j + \sum_{i>j} D_{i,j}(s_i^x s_j^y - s_i^y s_j^x) + \mu_B B\sum_i g_i s_i^z \quad (2)$$

where the first term represents the (leading) isotropic exchange interaction between different ions connected by red lines in Figure 1a with coupling strength $J_{i,j}$; the second is the axial Dzyaloshinskii−Moriya interaction (DMI), parametrized by $D_{i,j}$; and the latter is the Zeeman coupling of each ion with an external magnetic field parallel to z. For simplicity, we have assumed isotropic g_i factors and only axial terms in Hamiltonian 2. In the case of isosceles triangles at top and bottom with all their vertices coupled with the same strength to the center, the energies of the isotropic exchange multiplets can be analytically computed (see the Supporting Information). This allows us to identify a proper regime of parameters to get several low-energy multiplets with minimum total spin S

https://doi.org/10.1021/acs.jpclett.2c01602
J. Phys. Chem. Lett. 2022, 13, 6468−6474

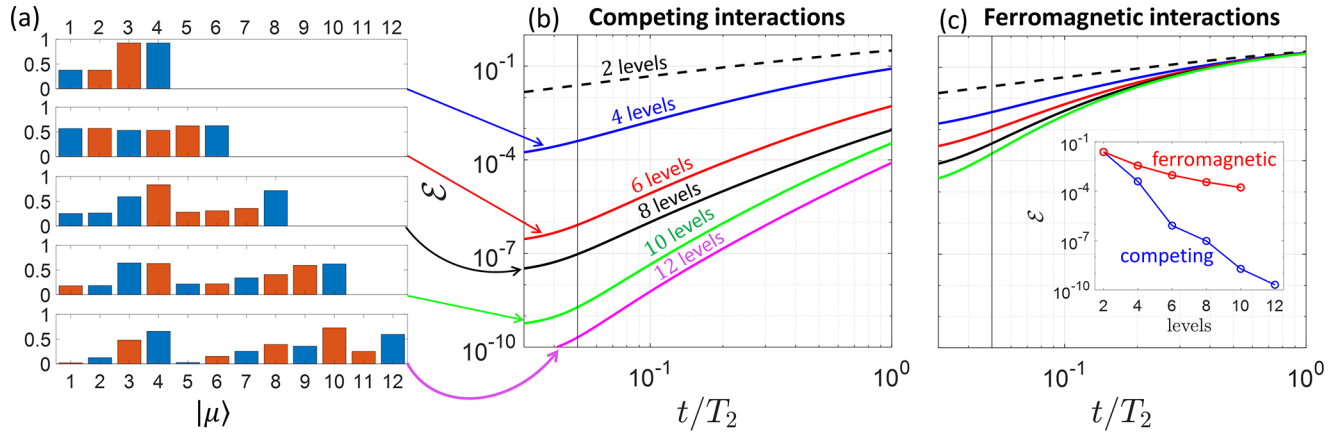

Figure 2. Quantum error correction using a properly designed molecular qudit. (a) Absolute value of the component of each code word on the eigenstates of **C**, labeled in the horizontal axis by a number from 1 to 12. Blue (orange) bars refer to $|0_L\rangle$ ($|1_L\rangle$). (b and c) Error $\mathcal{E} = 1 - \langle\psi_0|\rho|\psi_0\rangle$ after a memory time t in the molecular system of Figure 1a with competing (b) vs ferromagnetic (c) exchange interactions, exploiting an increasing number of levels for the encoding and starting from the error-prone state $|\psi_0\rangle = (|0_L\rangle + |1_L\rangle)/\sqrt{2}$. The code words are derived at $t/T_2 = 0.05$ (vertical line). The comparison shows an impressive gain in panel b compared to panel c, increasing with the number of levels up to 5 orders of magnitude (inset of panel c) at $t/T_2 = 0.05$.

= 1/2. In particular, by choosing positive (antiferromagnetic) values for all $J_{i,j}$ and the intratriangles coupling substantially larger than the coupling with the center, the spectrum displays eight doublets significantly separated from the first excited S = 3/2. This leads to a situation close to spin frustration,[34] with the degeneracy of the ground state removed by using slightly different $J_{i,j}$, as listed in the caption of Figure 1. This is the typical situation found in real molecules, which are usually not completely regular,[30−33,35−41] and is exactly our target, because such a symmetry breaking makes all transitions addressable in principle by resonant pulses (see the Supporting Information). Finally, DMI is exploited to couple to first order all different multiplets, thus providing matrix elements for direct transitions. We fix $D_{i,j} = J_{i,j}/10$, a reasonable assumption for, e.g., Cu^{2+} spin 1/2 ions with $g_i \approx 2.1-2.3$; see ref 42.

To quantitatively show that this system with *competing* interactions (**C**) fulfils the aforementioned requirements, we consider its lowest eigenstates and compute expectation values of local spin operators. In particular, we compare it with an isostructural molecule in which the sign of all $J_{i,j}$ is reversed, leading to an S = 9/2 ground multiplet (referred to hereafter as *ferromagnetic*, **F**). The latter perfectly matches the spin S cases examined previously,[21,22,43] but in the same bath of **C**. The average local spin moment over different sites $\langle m_z\rangle = \sum_i \langle s_i^z\rangle/7s_i$ is reported in Figure 1b for different eigenstates (a single one per Kramers pair). In the case of **F** and within the S = 9/2 ground multiplet, $|\mu\rangle \equiv |m\rangle$, where $|m\rangle$ are the common eigenstates of H and $S_z = \sum_i s_i^z$, $S_z|m\rangle = m|m\rangle$. Hence, one can easily find $\langle m|s_j^z|m\rangle = m/9$. This results in a strong variation of $\langle m_z\rangle$ among different eigenstates (red symbols), in contrast to the case of **C**, where $\langle m_z\rangle$ is very weakly dependent on the state. This is also evident from panel c, where we report the detailed distribution of $\langle s_i^z\rangle/s_i$ in **C** over different sites, showing again small values with a rather uniform distribution on the eigenstates. The different dependence of $\langle m_z\rangle$ on the examined eigenstate translates into a very different coherence decay. This is highlighted in Figure 1d, where we compare the fidelity decay of different superpositions of the 10 lowest states for **F** and **C**. The larger the variation of $\langle m_z\rangle$ in panel b, the faster the decay. This can be easily understood for **F**, in which case $\gamma_{mm'} = (m - m')^2/T_2$, where we have introduced an effective coherence rate $T_2^{-1} \propto \sum_{jj'=1}^{7} C_{jj'}^{zz}$, containing information on the bath and common to both **F** and **C**. All in all, Figure 1 provides insight into the crucial ingredients driving decoherence and illustrates our recipe to suppress it and to avoid its growth with the number of states by properly engineering the couplings in Hamiltonian 2.

Deriving Optimal Code Words. Building on the above model of decoherence, we show how to derive a hardware-efficient quantum error correction code capable of substantially suppressing errors. This is achieved in two steps. First, we focus on the d lowest levels of the system and we decompose ρ at time t through a set of operators E_k in this subspace:

$$\rho_t = \sum_{k=0}^{d-1} E_k \rho_0 E_k^\dagger \tag{3}$$

Starting from the solution of the Lindblad equation $\rho_{\mu\nu}(t) = e^{-\gamma_{\mu\nu}t}\rho_{\mu\nu}(0)$, the d independent diagonal E_k operators are derived through state tomography (see the Supporting Information and ref 44). The second step consists of identifying logical states (*code words*) $|0_L\rangle$ and $|1_L\rangle$, i.e., proper superpositions of the system eigenstates satisfying Knill−Laflamme conditions[45] on the subset of leading $d/2$ error operators $\{E_k\}$:[51]

$$\langle 0_L|E_k^\dagger E_j|0_L\rangle = \langle 1_L|E_k^\dagger E_j|1_L\rangle$$
$$\langle 0_L|E_k^\dagger E_j|1_L\rangle = 0 \tag{4}$$

The second condition is guaranteed by choosing different $|\mu\rangle$ states to define $|0_L\rangle$ and $|1_L\rangle$, being all E_k diagonal. The first one leads to a linear system of equations for the squared coefficients of the logical states on the $|\mu\rangle$ basis of states, for which at least one solution can be found, either by matrix pseudoinversion or by numerical optimization (see the Supporting Information). Figure 2a shows as a bar plot the absolute value of the components on each eigenstate of the code words (derived at t/T_2 = 0.05) for **C**.

https://doi.org/10.1021/acs.jpclett.2c01602
J. Phys. Chem. Lett. 2022, 13, 6468−6474

To test the performance of the optimized code words, we perform an ideal QEC cycle applied after memory time t. This is done by starting from a generic superposition state $|\psi_0\rangle = \alpha|0_L\rangle + \beta|1_L\rangle$ and letting the system evolve freely (only subject to decoherence) for time t. Then, we check if each of the E_k errors has occurred by projecting the state of the system into one of the $d/2$ error words $\{|e_k^0\rangle, |e_k^1\rangle\}$, i.e., an orthonormal set of states spanning the same Hilbert space as $\{E_k|0_L\rangle, E_k|1_L\rangle\}$.[21] Thanks to the structure of the code words which satisfy eq 4, the resulting state $\alpha|e_k^0\rangle + \beta|e_k^1\rangle$ still preserves the initially stored information. Hence, we can finally apply the corresponding recovery operation $\alpha|e_k^0\rangle + \beta|e_k^1\rangle \rightarrow \alpha|0_L\rangle + \beta|1_L\rangle$ to restore the logical state. Results of this procedure are reported in Figure 2b,c. As expected, the error $\mathcal{E} = 1 - \mathcal{F}$ is dramatically lower in **C** (b) compared to **F** (c). This is also evidenced in the inset, where $\mathcal{E}$ is shown as a function of the number of levels used for the encoding. In moving from **F** to **C**, $\mathcal{E}$ is suppressed up to 5 orders of magnitude with 10 levels (the maximum number for a $S = 9/2$ multiplet). In principle, the error could be further reduced by deriving code words at shorter times and/or including a larger number of levels in the encoding.

Benchmarking Quantum Error Correction. The actual implementation of QEC requires a further step: a clear scheme to identify, measure, and correct errors. Here we present efficient strategies to achieve this, exploiting the peculiar structure of the eigenstates of **C**. The simplest one is based on measuring directly the state of the qudit, which can be done on the basis of the system eigenstates $|\mu\rangle$. However, the system is in general in a superposition of different eigenstates and of different error words. Hence, in order to perform a measurement that distinguishes different errors we need to map each error word $\alpha|e_k^0\rangle + \beta|e_k^1\rangle$ into a specific pair of system eigenstates $\alpha|\mu_0\rangle + \beta|\mu_1\rangle$. Such a mapping can be directly achieved by a sequence of parallel pulses thanks to the connectivity between the energy levels, which enables direct transitions among all of them. Then, simultaneous measurement of the pair of levels $|\mu_l\rangle$ ($l = 0,1$) allows one to identify the error word without collapsing the encoded state[21,22] and to apply the corresponding recovery.

This procedure hides, however, a potential drawback: by mapping each error word into a specific eigenstate (*decoding*), we leave the protected state for some time. To avoid this, we propose an alternative error detection scheme, in which measurements are performed on the eigenstates of an ancillary $d/2$-level qudit (e.g., a single electronic or nuclear spin or another molecule), which flag each of the $d/2$ errors E_k. The idea is to apply a sequence of pulses, detailed in the circuit of Figure 3a and in the Supporting Information, entangling system and ancilla in such a way that in the output superposition each state of the ancilla is in one-to-one correspondence with one of the error words (and hence, in practice, with one of the errors E_k). Then, by measuring the ancilla in its eigenbasis we project the state of the logical qudit into a specific error word and we can apply the corresponding recovery R_k.

The sequence of operations outlined in Figure 3a requires conditional ancilla−qudit U_k gates. Their implementation by microwave pulses requires distinguishing excitations of **C**, depending on each state of the ancilla. This, in turn, implies a sufficient qudit−ancilla coupling to spectroscopically resolve all of them. Then, each unitary U_k is implemented by two sets of

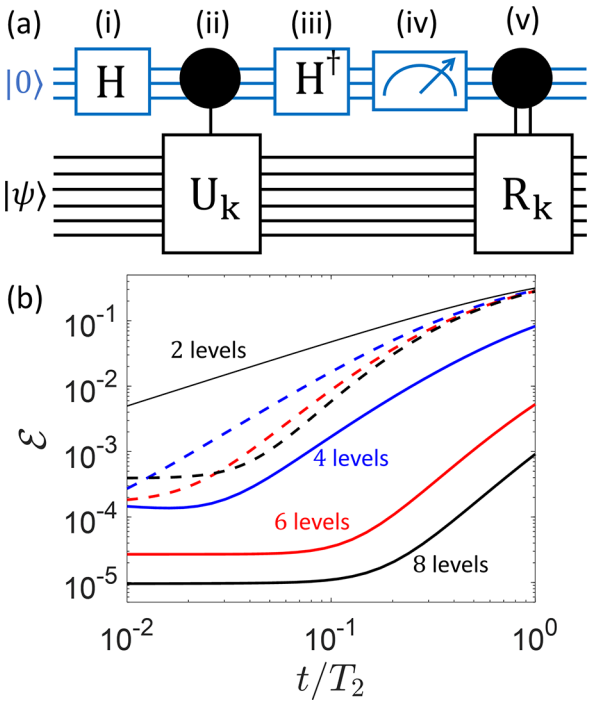

Figure 3. (a) Quantum circuit to detect error E_k on a d level qudit (bottom black lines), exploiting a $d/2$ level qudit ancilla (top blue lines): Starting with the ancilla in the ground state $|0\rangle$ and the logical qudit in $|\psi_0\rangle = \alpha|0_L\rangle + \beta|1_L\rangle$, we first (i) prepare the ancilla in a uniform superposition of its $d/2$ levels (through a generalized Hadamard gate H). Then, (ii) we implement a different unitary evolution U_k (one for each error E_k) on the logical qudit, conditioned by each of the $|k\rangle$ eigenstates of the ancilla. Next, (iii) we apply the inverse of transformation (i) to the ancilla and (iv) measure its state, projecting the system into a specific error word. Finally, a (v) specific recovery R_k is applied, depending on the measurement outcome. (b) Resulting error after a memory time t/T_2, using the whole pulse sequence to detect and correct errors and exploiting an increasing number of levels for the encoding. Here, $T_2 = 10^5\tau$, with τ being the largest time required to implement an elementary π pulse. Continuous (dashed) lines refer to **C** (**F**).

simultaneous pulses while always keeping the system encoded, as detailed in the Supporting Information. The state of the ancilla can be finally read out by coupling it to a superconducting resonator and measuring its frequency shift.[46] Remarkably, thanks to the full connectivity between energy levels ensured by the DMI in Hamiltonian 2, the length of the sequence does not increase with the number of states.

This, combined with the suppression of decoherence, yields a much better performance than **F**, as can be seen by comparing solid and dashed lines in Figure 3b. In particular, the error at short t/T_2 increases in **F** by increasing the number of levels, due to both the growth of decoherence and of the number of pulses to implement the correction.[21] In contrast, **C** shows a reduction of $\mathcal{E}$ by increasing d.[52] The reported numerical simulations include the whole pulse sequence and the effect of pure dephasing on the qudit, but we assume perfect pulses (with no leakage to neighboring levels). Indeed, pulse imperfections strongly depend on specific details of the system Hamiltonian and of the experimental apparatus and could be significantly suppressed by optimal quantum control techniques,[47] which is beyond the scope of the present work. Using the spin Hamiltonian parameters listed above (chosen to well resolve all the transitions), electron paramagnetic

https://doi.org/10.1021/acs.jpclett.2c01602
J. Phys. Chem. Lett. 2022, 13, 6468−6474

resonance frequencies up to the W-band are needed. However, we stress that by using optimal quantum control to shape pulses these frequencies could be reduced (e.g., by an overall reduction of the coupling in Hamiltonian 2) without significantly affecting gate fidelities. Targeting molecules with smaller couplings would also be advantageous to decrease the rate of spin−lattice processes, in case phonon-induced relaxation turned out to be disturbing. Yet, such an effect is expected to be minor. For example, for the frustrated Cu_3 triangle studied in ref 48, T_1 values as large as hundreds of microseconds were observed, in spite of gaps much bigger than in our case.

Protected Quantum Gates. The total connectivity between the energy levels involved in the encoding also allows us to design a scheme to implement generic $R_\alpha(\vartheta)$ logical gates between encoded states. We focus here on the more demanding planar rotations $R_{x,y}$, because diagonal one- and two-qubit gates can be implemented more easily.[43] These are obtained by inducing simultaneous transitions between each component of $|0_L\rangle$ and those of $|1_L\rangle$, without decoding (i.e., mapping each logical state into a single level). In contrast, implementing the same gate on **F** would require a long sequence of pulses, practically equivalent to decoding, applying the rotation, and encoding again. As a result, the performance of **C** is much better already for a $d = 4$ qudit, as highlighted in Figure 4. Here we report numerical simulations of a sequence of $R_x(\pi)$ rotations, followed by a short memory time (as it would happen in a complex algorithm) and by a QEC cycle. While the final error in **F** (red crosses) is always larger than that on a not protected spin 1/2 qubit (dashed line), **C** reveals a significant advantage (blue symbols), even with application of the full pulse sequence (circles). This translates into a gain (panel b) compared to the spin 1/2 approaching 4 after implementation of 30 gates, which is remarkable having exploited the qudit with minimum protection, namely, $d = 4$.

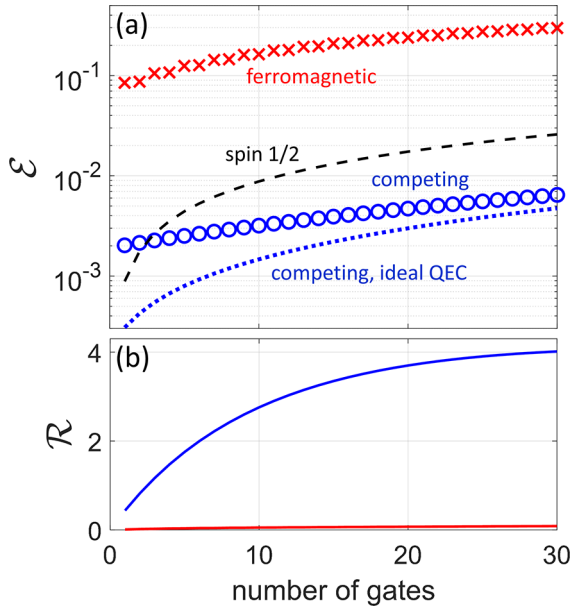

Figure 4. Protected quantum gates on a four-level qudit. Error $\mathcal{E}$ (a) and gain $\mathcal{R}$ compared to an uncorrected spin 1/2 (i.e. ratio between errors in the un-corrected and corrected cases) (b) in the implementation of a sequence of $R_x(\pi)$ rotations of the logical qubit of duration τ, each one followed by a memory time 2τ and by a QEC cycle. Blue circles (red crosses) refer to **C** (**F**). In the former case, the connectivity between the system eigenstates allows us to perform generic $R_x(\vartheta)$ rotations much faster and without decoding, resulting in a much better performance. Blue dots are the result of a noisy gate, followed by an ideal QEC cycle, while the dashed line is the error for an uncorrected qubit, subject to the same gate and memory time. In the simulations, leakage is neglected and we assume $T_2 = 10^3\tau$.

In summary, we have theoretically designed molecular nanomagnets showing a striking performance as qubits with embedded quantum error correction. This is achieved through an insight into the role of the spin structure of the eigenstates on the mechanisms ruling decoherence, which allowed us to identify as optimal units multispin molecules with competing exchange interactions. Indeed, these systems are characterized by several low-energy multiplets where decoherence is strongly suppressed and does not grow with the number of levels in the encoding. In this respect, one could also engineer molecular systems embedding an increasingly large number of long-coherence states at low energy.[33,34] In addition, these levels are directly connected by microwave transitions. These two features allow us to derive protected logical states and to design efficient pulse sequences to actually implement quantum error correction and quantum gates.

■ ASSOCIATED CONTENT

Supporting Information

The Supporting Information is available free of charge at https://pubs.acs.org/doi/10.1021/acs.jpclett.2c01602.

Details on the energy spectrum of the examined systems, derivation of the master equation, state tomography and determination of the code words, pulse sequence to implement quantum error correction and logical gates (PDF)

■ AUTHOR INFORMATION

Corresponding Authors

A. Chiesa − *Università di Parma, Dipartimento di Scienze Matematiche, Fisiche e Informatiche, I-43124 Parma, Italy; Gruppo Collegato di Parma, INFN−Sezione di Milano-Bicocca, 43124 Parma, Italy; UdR Parma, INSTM, I-43124 Parma, Italy;* orcid.org/0000-0003-2955-3998; Email: alessandro.chiesa@unipr.it

S. Carretta − *Università di Parma, Dipartimento di Scienze Matematiche, Fisiche e Informatiche, I-43124 Parma, Italy; Gruppo Collegato di Parma, INFN−Sezione di Milano-Bicocca, 43124 Parma, Italy; UdR Parma, INSTM, I-43124 Parma, Italy;* orcid.org/0000-0002-2536-1326; Email: stefano.carretta@unipr.it

Authors

F. Petiziol − *Institut für Theoretische Physik, Technische Universität Berlin, 10623 Berlin, Germany*

M. Chizzini − *Università di Parma, Dipartimento di Scienze Matematiche, Fisiche e Informatiche, I-43124 Parma, Italy; Gruppo Collegato di Parma, INFN−Sezione di Milano-Bicocca, 43124 Parma, Italy*

P. Santini − *Università di Parma, Dipartimento di Scienze Matematiche, Fisiche e Informatiche, I-43124 Parma, Italy; Gruppo Collegato di Parma, INFN−Sezione di Milano-Bicocca, 43124 Parma, Italy; UdR Parma, INSTM, I-43124 Parma, Italy*

Complete contact information is available at:

https://doi.org/10.1021/acs.jpclett.2c01602
J. Phys. Chem. Lett. 2022, 13, 6468−6474

https://pubs.acs.org/10.1021/acs.jpclett.2c01602

Notes

The authors declare no competing financial interest.

■ ACKNOWLEDGMENTS

This work received financial support from the European Union's Horizon 2020 program under Grant Agreement No. 862893 (FET-OPEN project FATMOLS). F.P. was funded by the Deutsche Forschungsgemeinschaft (DFG, German Research Foundation) Projektnummer 163436311 SFB 910.

■ REFERENCES

(1) Bruzewicz, C. D.; Chiaverini, J.; McConnell, R.; Sage, J. M. Trapped-Ion Quantum Computing: Progress and Challenges. *Appl. Phys. Rev.* **2019**, *6*, 021314.
(2) Zhong, H.-S.; et al. Quantum Computational Advantage Using Photons. *Science* **2020**, *370*, 1460−1463.
(3) Arrazola, J. M.; et al. Quantum Circuits with Many Photons on a Programmable Nanophotonic Chip. *Nature* **2021**, *591*, 54−60.
(4) Blais, A.; Grimsmo, A. L.; Girvin, S. M.; Wallraff, A. Circuit Quantum Electrodynamics. *Rev. Mod. Phys.* **2021**, *93*, 025005.
(5) Tacchino, F.; Chiesa, A.; Carretta, S.; Gerace, D. Quantum Computers as Universal Quantum Simulators: State-of-Art and Perspectives. *Adv. Quantum Technol.* **2020**, *3*, 1900052.
(6) Arute, F.; et al. Quantum Supremacy Using a Programmable Superconducting Processor. *Nature* **2019**, *574*, 505−510.
(7) Arute, F.; et al. Hartree-Fock on a Superconducting Qubit Quantum Computer. *Science* **2020**, *369*, 1084−1089.
(8) Hendrickx, N. W.; Lawrie, W. I. L.; Russ, M.; Riggelen, F. v.; de Snoo, S. L.; Schouten, R. N.; Sammak, A.; Scappucci, G.; Veldhorst, M. A Four-Qubit Germanium Quantum Processor. *Nature* **2021**, *591*, 580−585.
(9) Chatterjee, A.; Stevenson, P.; De Franceschi, S.; Morello, A.; de Leon, N. P.; Kuemmeth, F. Semiconductor Qubits in Practice. *Nat. Rev. Phys.* **2021**, *3*, 157−177.
(10) Chiesa, A.; Tacchino, F.; Grossi, M.; Santini, P.; Tavernelli, I.; Gerace, D.; Carretta, S. Quantum Hardware Simulating Four-Dimensional Inelastic Neutron Scattering. *Nat. Phys.* **2019**, *15*, 455−459.
(11) Terhal, B. M. Quantum Error Correction for Quantum Memories. *Rev. Mod. Phys.* **2015**, *87*, 307−342.
(12) Devitt, S. J.; Munro, W. J.; Nemoto, K. Quantum Error Correction for Beginners. *Rep. Prog. Phys.* **2013**, *76*, 076001.
(13) Fowler, A. G.; Mariantoni, M.; Martinis, J. M.; Cleland, A. N. Surface Codes: Towards Practical Large-Scale Quantum Computation. *Phys. Rev. A* **2012**, *86*, 032324.
(14) Shiddiq, M.; Komijani, D.; Duan, Y.; Gaita-Ariño, A.; Coronado, E.; Hill, S. Enhancing Coherence in Molecular Spin Qubits via Atomic Clock Transitions. *Nature* **2016**, *531*, 348−351.
(15) Gaita-Ariño, A.; Luis, F.; Hill, S.; Coronado, E. Molecular Spins for Quantum Computation. *Nat. Chem.* **2019**, *11*, 301−309.
(16) Atzori, M.; Sessoli, R. The Second Quantum Revolution: Role and Challenges of Molecular Chemistry. *J. Am. Chem. Soc.* **2019**, *141*, 11339−11352.
(17) Rugg, B. K.; Krzyaniak, M. D.; Phelan, B. T.; Ratner, M. A.; Young, R. M.; Wasielewski, M. R. Photodriven Quantum Teleportation of an Electron Spin State in a Covalent Donor−Acceptor−Radical System. *Nat. Chem.* **2019**, *11*, 981−986.
(18) Wasielewski, M. R.; Forbes; Frank, N. L.; Kowalski, K.; Scholes, G. D.; Yuen-Zhou, J.; Baldo, M. A.; Freedman, D. E.; Goldsmith, R. H.; Goodson, T.; Kirk, M. L.; McCusker, J. K.; Ogilvie; Shultz, D. A.; Stoll, S.; Whaley, K. B. Exploiting Chemistry and Molecular Systems for Quantum Information Science. *Nat. Rev. Chem.* **2020**, *4*, 490−504.
(19) Carretta, S.; Zueco, D.; Chiesa, A.; Gómez-León, A.; Luis, F. A Perspective on Scaling up Quantum Computation with Molecular Spins. *Appl. Phys. Lett.* **2021**, *118*, 240501.
(20) Liu, J.; Mrozek, J.; Ullah, A.; Duan, Y.; Baldoví, J. J.; Coronado, E.; Gaita-Ariño, A.; Ardavan, A. Quantum Coherent Spin−Electric Control in a Molecular Nanomagnet at Clock Transitions. *Nat. Phys.* **2021**, *17*, 1205−1209.
(21) Chiesa, A.; Macaluso, E.; Petiziol, F.; Wimberger, S.; Santini, P.; Carretta, S. Molecular Nanomagnets as Qubits with Embedded Quantum-Error Correction. *J. Phys. Chem. Lett.* **2020**, *11*, 8610−8615.
(22) Petiziol, F.; Chiesa, A.; Wimberger, S.; Santini, P.; Carretta, S. Counteracting Dephasing in Molecular Nanomagnets by Optimized Qudit Encodings. *npj Quantum Inf* **2021**, *7*, 133.
(23) Bader, K.; Dengler, D.; Lenz, S.; Endeward, B.; Jiang, S.-D.; Neugebauer, P.; van Slageren, J. Room Temperature Quantum Coherence in a Potential Molecular Qubit. *Nat. Commun.* **2014**, *5*, 5304.
(24) Yu, C.-J.; Graham, M. J.; Zadrozny, J. M.; Niklas, J.; Krzyaniak, M. D.; Wasielewski, M. R.; Poluektov, O. G.; Freedman, D. E. Long Coherence Times in Nuclear Spin-Free Vanadyl Qubits. *J. Am. Chem. Soc.* **2016**, *138*, 14678−14685.
(25) Moreno-Pineda, E.; Godfrin, C.; Balestro, F.; Wernsdorfer, W.; Ruben, M. Molecular Spin Qudits for Quantum Algorithms. *Chem. Soc. Rev.* **2018**, *47*, 501−513.
(26) Biard, H.; Moreno-Pineda, E.; Ruben, M.; Bonet, E.; Wernsdorfer, W.; Balestro, F. Increasing the Hilbert Space Dimension Using a Single Coupled Molecular Spin. *Nat. Commun.* **2021**, *12*, 4443.
(27) Lockyer, S. J.; Chiesa, A.; Timco, G. A.; McInnes, E. J. L.; Bennett, T. S.; Vitorica-Yrezebal, I. J.; Carretta, S.; Winpenny, R. E. P. Targeting Molecular Quantum Memory with Embedded Error Correction. *Chem. Sci.* **2021**, *12*, 9104−9113.
(28) Chicco, S.; Chiesa, A.; Allodi, G.; Garlatti, E.; Atzori, M.; Sorace, L.; De Renzi, R.; Sessoli, R.; Carretta, S. Controlled Coherent Dynamics of [VO(TPP)], a Prototype Molecular Nuclear Qudit with an Electronic Ancilla. *Chem. Sci.* **2021**, *12*, 12046−12055.
(29) Gimeno, I.; Urtizberea, A.; Román-Roche, J.; Zueco, D.; Camón, A.; Alonso, P. J.; Roubeau, O.; Luis, F. Broad-Band Spectroscopy of a Vanadyl Porphyrin: a Model Electronuclear Spin Qudit. *Chem. Sci.* **2021**, *12*, 5621−5630.
(30) Garlatti, E.; Carretta, S.; Affronte, M.; Sanudo, E. C.; Amoretti, G.; Santini, P. Magnetic Properties and Relaxation Dynamics of a Frustrated Ni_7 Molecular Nanomagnet. *J. Phys.: Cond. Matt.* **2012**, *24*, 104006.
(31) Baker, M. L.; et al. Studies of a Large Odd-Numbered Odd-Electron Metal Ring: Inelastic Neutron Scattering and Muon Spin Relaxation Spectroscopy of Cr_8Mn. *Chem.—Eur. J.* **2016**, *22*, 1779−1788.
(32) Woolfson, R. J.; Timco, G. A.; Chiesa, A.; Vitorica-Yrezabal, I. J.; Tuna, F.; Guidi, T.; Pavarini, E.; Santini, P.; Carretta, S.; Winpenny, R. E. P. [CrF(O2CtBu)2]9: Synthesis and Characterization of a Regular Homometallic Ring with an Odd Number of Metal Centers and Electrons. *Angew. Chem., Int. Ed.* **2016**, *55*, 8856−8859.
(33) van Slageren, J.; Rosa, P.; Caneschi, A.; Sessoli, R.; Casellas, H.; Rakitin, Y. V.; Cianchi, L.; Giallo, F. D.; Spina, G.; Bino, A.; Barra, A.-L.; Guidi, T.; Carretta, S.; Caciuffo, R. Static and Dynamic Magnetic Properties of an $[Fe_{13}]$ Cluster. *Phys. Rev. B* **2006**, *73*, 014422.
(34) Schnack, J. Effects of Frustration on Magnetic Molecules: a Survey from Olivier Kahn until Today. *Dalton Trans* **2010**, *39*, 4677−4686.
(35) Antkowiak, M.; Kozłowski, P.; Kamieniarz, G.; Timco, G. A.; Tuna, F.; Winpenny, R. E. P. Detection of Ground States in Frustrated Molecular Rings by in-Field Local Magnetization Profiles. *Phys. Rev. B* **2013**, *87*, 184430.
(36) Garlatti, E.; Carretta, S.; Santini, P.; Amoretti, G.; Mariani, M.; Lascialfari, A.; Sanna, S.; Mason, K.; Chang, J.; Tasker, P.; Brechin, E. K. Relaxation Dynamics in a Fe_7 Nanomagnet. *Phys. Rev. B* **2013**, *87*, 054409.
(37) Baker, M.; et al. A Classification of Spin Frustration in Molecular Magnets From a Physical Study of Large Odd-Numbered-

https://doi.org/10.1021/acs.jpclett.2c01602
J. Phys. Chem. Lett. 2022, 13, 6468−6474

Metal, Odd Electron Rings. *Proc. Natl. Acad. Sci. U.S.A.* **2012**, *109*, 19113−19118.
(38) Florek, W.; Antkowiak, M.; Kamieniarz, G. Sequences of Ground States and Classification of Frustration in Odd-Numbered Antiferromagnetic Rings. *Phys. Rev. B* **2016**, *94*, 224421.
(39) Furukawa, Y.; Kiuchi, K.; Kumagai, K.-i.; Ajiro, Y.; Narumi, Y.; Iwaki, M.; Kindo, K.; Bianchi, A.; Carretta, S.; Santini, P.; Borsa, F.; Timco, G. A.; Winpenny, R. E. P. Evidence of Spin Singlet Ground State in the Frustrated Antiferromagnetic Ring Cr_8Ni. *Phys. Rev. B* **2009**, *79*, 134416.
(40) Ghirri, A.; Chiesa, A.; Carretta, S.; Troiani, F.; van Tol, J.; Hill, S.; Vitorica-Yrezabal, I.; Timco, G. A.; Winpenny, R. E. P.; Affronte, M. Coherent Spin Dynamics in Molecular Cr_8Zn Wheels. *J. Phys. Chem. Lett.* **2015**, *6*, 5062−5066.
(41) Adelnia, F.; Chiesa, A.; Bordignon, S.; Carretta, S.; Ghirri, A.; Candini, A.; Cervetti, C.; Evangelisti, M.; Affronte, M.; Sheikin, I.; Winpenny, R.; Timco, G.; Borsa, F.; Lascialfari, A. Low Temperature Magnetic Properties and Spin Dynamics in Single Crystals of Cr_8Zn antiferromagnetic molecular rings. *J. Chem. Phys.* **2015**, *143*, 244321.
(42) Choi, K.-Y.; Matsuda, Y. H.; Nojiri, H.; Kortz, U.; Hussain, F.; Stowe, A. C.; Ramsey, C.; Dalal, N. S. Observation of a Half Step Magnetization in the Cu_3-Type Triangular Spin Ring. *Phys. Rev. Lett.* **2006**, *96*, 107202.
(43) Chiesa, A.; Petiziol, F.; Macaluso, E.; Wimberger, S.; Santini, P.; Carretta, S. Embedded Quantum-Error Correction and Controlled-Phase Gate for Molecular Spin Qubits. *AIP Adv.* **2021**, *11*, 025134.
(44) Nielsen, M. A.; Chuang, I. L. *Quantum Computation and Quantum Information: 10th Anniversary Edition*; Cambridge University Press: Cambridge, 2011.
(45) Knill, E.; Laflamme, R. Theory of Quantum Error-Correcting Codes. *Phys. Rev. A* **1997**, *55*, 900−911.
(46) Gómez-León, A.; Luis, F.; Zueco, D. Dispersive Readout of Molecular Spin Qudits. *Phys. Rev. Applied* **2022**, *17*, 064030.
(47) Castro, A.; Garcia Carrizo, A.; Roca, S.; Zueco, D.; Luis, F. Optimal Control of Molecular Spin Qudits. *Phys. Rev. Applied* **2022**, *17*, 064028.
(48) Choi, K.-Y.; Wang, Z.; Nojiri, H.; van Tol, J.; Kumar, P.; Lemmens, P.; Bassil, B. S.; Kortz, U.; Dalal, N. S. Coherent Manipulation of Electron Spins in the Cu_3 Spin Triangle Complex Impregnated in Nanoporous Silicon. *Phys. Rev. Lett.* **2012**, *108*, 067206.
(49) Here we assume, for simplicity, an axial system with isotropic g_i. In this case, one gets $C_{jj'}^{\alpha\alpha'} \propto \sum_{nn'} \sum_{\beta\beta'} d_{jn}^{\alpha\beta} d_{j'n'}^{\alpha'\beta'}$, where $d_{jn}^{\alpha\beta} = g_j g_N \mu_B \mu_N (3 r_{jn}^{\alpha} r_{jn'}^{\beta} / |r_{jn}|^2 - \delta_{\alpha\beta}) / |r_{jn}|^3$, g_N is the nuclear spin spectroscopic factor, μ_N is the nuclear magneton and r_{jn}^{α} is the α component of the distance between the jth electronic spin and the nth nuclear spin. Numerical values are obtained by generating a random distribution of nuclear spins (Figure 1a).
(50) This could be addressed with many-body numerical methods such as a cluster-correlation expansion,[22] but it would prohibitively constrain the Hilbert-space dimensions accessible in numerical simulations because of the increased computational effort.
(51) $d/2$ E_k operators acting on $|0_L\rangle$ and $|1_L\rangle$ span the whole Hilbert space of dimension d. We therefore write Knill−Laflamme conditions for the leading $d/2$ error operators, which can be easily identified because our procedure leads to a clear hierarchy in their norm. Hence, $d/2$ operators are already enough to catch the correct dynamics.
(52) The residual error at short t/T_2 is due to pure dephasing acting during the implementation of the pulse sequence and inducing errors uncorrectable by the code.

https://doi.org/10.1021/acs.jpclett.2c01602
J. Phys. Chem. Lett. 2022, 13, 6468−6474